JACS
JOURNAL OF THE AMERICAN CHEMICAL SOCIETY
pubs.acs.org/JACS
Article

Stabilization of Lead-Reduced Metal Halide Perovskite Nanocrystals by High-Entropy Alloying

Simon F. Solari,[#] Lok-Nga Poon,[#] Michael Wörle, Frank Krumeich, Yen-Ting Li, Yu-Cheng Chiu, and Chih-Jen Shih*

Cite This: J. Am. Chem. Soc. 2022, 144, 5864–5870
Read Online
ACCESS | Metrics & More | Article Recommendations | Supporting Information

ABSTRACT: Colloidal metal halide perovskite (MHP) nanocrystals (NCs) are an emerging class of fluorescent quantum dots (QDs) for next-generation optoelectronics. A great hurdle hindering practical applications, however, is their high lead content, where most attempts addressing the challenge in the literature compromised the material's optical performance or colloidal stability. Here, we present a postsynthetic approach that stabilizes the lead-reduced MHP NCs through high-entropy alloying. Upon doping the NCs with multiple elements in considerably high concentrations, the resulting high-entropy perovskite (HEP) NCs remain to possess excellent colloidal stability and narrowband emission, with even higher photoluminescence (PL) quantum yields, η_{PL}, and shorter fluorescence lifetimes, τ_{PL}. The formation of multiple phases containing mixed interstitial and doping phases is suggested by X-ray crystallography. Importantly, the crystalline phases with higher degrees of lattice expansion and lattice contraction can be stabilized upon high-entropy alloying. We show that the lead content can be approximately reduced by up to 55% upon high-entropy alloying. The findings reported here make one big step closer to the commercialization of perovskite NCs.

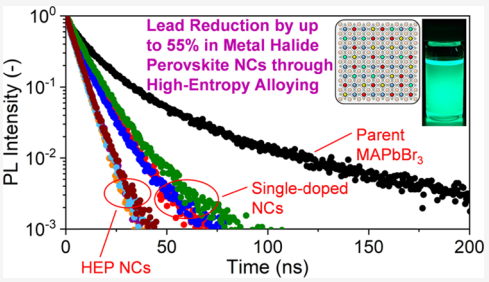

INTRODUCTION

Metal halide perovskites (MHPs), with the general formula of ABX_3, where A is a monovalent organic/inorganic cation, B is a divalent metal cation, and X is a halide anion, have generated considerable research efforts aimed at demonstrating their outstanding optical properties.[1−3] The most studied compounds of this family are based on lead, with the general formula $APbX_3$, because of their defect tolerance that originated from the shallowly populated defect states near the band edges. This unique property enables the $APbX_3$ nanocrystals to possess very high photoluminescence (PL) quantum yields, η_{PL}, and narrowband emission, which give rise to high-efficiency optoelectronic devices, including photovoltaics (PVs),[4,5] photodetectors,[6] and light-emitting diodes (LEDs).[7−10]

The actual implementation of $APbX_3$ NCs in photonic devices toward commercialization, however, has faced a number of challenges. Inarguably, the greatest one is about the toxicity of lead.[11] Following the development of lead-free MHP PVs, divalent cations with similar ionic radii, such as Sn^{2+} or Eu^{2+}, were examined.[12,13] However, most lead-free perovskite NCs either compromised their optical properties or colloidal stability.[14−16] Accordingly, lead-reduced MHPs,[17−19] in which the B-site lead ions are partially replaced, have become increasingly attractive.[20,21] Lead-reduced MHP NCs have been synthesized using the hot-injection (HI) method,[17,22−30] where a complex reaction setup is required, as well as the postsynthetic approaches by doping with Mg^{2+}, Mn^{2+}, Sn^{2+}, Cd^{2+}, and Zn^{2+}.[19,31−33] It is noted that the latter approach had rather limited success as compared to the postsynthetic A- and X-site mixing owing to the structural rigidity of PbX_6^{4-} octahedron.[34] For example, it has been shown that one can only add a relatively small amount of secondary elements in the $CsPb_{1-x}M_xBr_3$ perovskite NCs (M = Sn^{2+}, Cd^{2+}, or Zn^{2+}; $0 < x \leq 0.1$).[32] To our knowledge, it is not yet possible to significantly increase the content of secondary B-site ions without compromising the production yield and optical performance.

From a fundamental point of view, the partial replacement of lead ions in perovskite lattices is analogous to alloying, which has long been used to alter material properties. Traditional alloying usually refers to the addition of relatively small amounts of secondary elements to a primary element. Intriguingly, recent advance in high-entropy alloys (HEAs) suggests that the combination of multiple principal elements in high concentrations could increase the configurational entropy of mixing that overcomes the enthalpies of compound

Received: November 22, 2021
Published: March 23, 2022

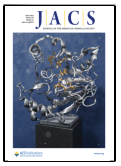

https://doi.org/10.1021/jacs.1c12294
J. Am. Chem. Soc. 2022, 144, 5864−5870

formation, thereby stabilizing the HEAs.[35−37] Very recently, A-site doping of lead halide perovskite (LHP) NCs has shown to improve the optical properties and chemical stability due to the entropy of mixing.[38,39] Back to the 2010s, high-entropy perovskite materials, including high-entropy perovskite oxides (HEPOs) and high-entropy perovskite fluorides (HEPFs) had emerged.[40−43] These high-entropy perovskite compounds have demonstrated outstanding catalytic properties, serving as efficient electrocatalysts in the oxygen evolution reaction.[43,44] The preparation of HEPOs, however, demands a process temperature of greater than 1000 °C.[40−42,45] Clearly, it is desirable to develop less energy-consuming approaches for the synthesis of high-entropy perovskite materials.

Inspired by the underlying principle of high-entropy alloying, we hypothesized that the entropy of mixing could favor the stabilization of lead-reduced perovskite NCs by mixing with multiple secondary B-site elements, termed the high-entropy perovskites (HEPs). In this report, we synthesized the HEP NCs for the first time and investigated their optical, crystallographic, and compositional characteristics.

RESULTS AND DISCUSSION

The HEP NCs were synthesized using a modified protocol developed by our group to overcome the solubility difference between precursors, namely, the ligand-assisted solid-phase synthesis (LASPS).[46] First, the parent colloidal $MAPbBr_3$ NCs were prepared and dispersed in toluene ($MA^+ = CH_3NH_3^+$). The NC solution was then stirred with an excess solid powder mixture of metal bromides, MBr_2 ($M = Mg^{2+}$, Zn^{2+}, and Cd^{2+}), and a small amount of long-chain organic surfactants, such as oleic acid and oleylamine, forming dynamic binding on the NC surface.[47] The surfactants assist gradual dissolution of MBr_2 solid powders by forming inverse micelles that increase the chemical potentials of secondary metal elements in solution, thereby slowly replacing lead in NCs. Metal bromide salts were chosen to prevent undesirable halide exchange.[48] Each reaction was performed under magnetic stirring in nitrogen at room temperature for several hours to reach saturation of solid solubility, followed by removing excess surfactants and MBr_2 by a number of polar solvents, such as methyl acetate, acetonitrile, and ethanol.

The protocol presented here allows us easy access to the compositional space without taking into account the solubility limit of metal precursors in antisolvents, which is cumbersome in many HI and postsynthetic approaches, particularly suitable for studying the HEPs and their synthesis (Figure 1a). We noticed that the protocol developed here highly preserved the solution optical density, which is demonstrated by the photographs of the synthesized colloidal solutions under UV excitation, in which we label each sample with the B-site elements, for example, PbZnCd for $MA(PbZnCd)Br_3$ HEP NCs, all yielding strong fluorescence (Figure 1b).

As compared to parent $MAPbBr_3$, the synthesized single-doped perovskite NCs and the HEP NCs exhibit different degrees of blueshift in their PL and absorption spectra (Figure 2a and Supplementary Figure S1), with the emission bandwidth remaining nearly unchanged. A possible explanation for the observed blueshift is the lattice contraction of the perovskite unit cell upon alloying.[32] Surprisingly, upon alloying, the η_{PL} value increases from ∼75% to up to ∼95% (Figure 2b), together with a decrease in the average PL lifetime value, τ_{avg}, from 27.3 ns to as low as 4.6 ns (Figure 2c). More notably, there seemed a stepwise trend that the fluorescence

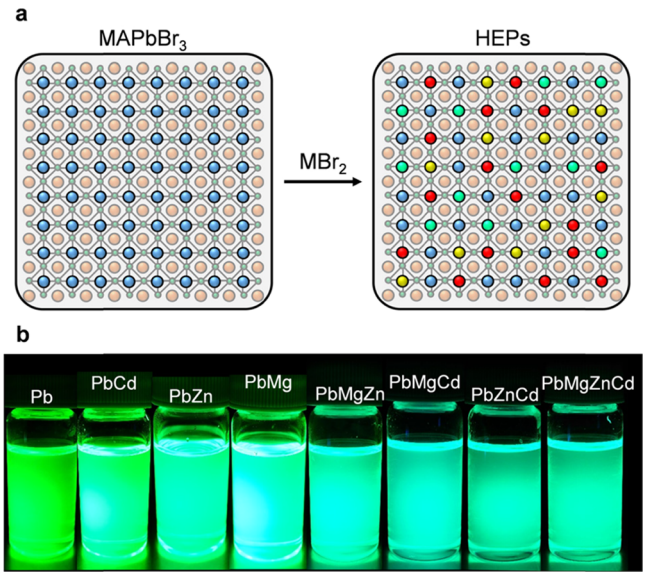

Figure 1. Synthesis of HEP NCs. (a) Schematic diagram showing a possible reaction that occurs when three additional elements are doped in the perovskite lattice upon mixing with a metal halide powder blend. (b) Representative photographs of synthesized colloidal solutions under UV excitation. Each sample is labeled with the B-site elements, for example, PbZnCd for $MA(PbZnCd)Br_3$ HEP NCs.

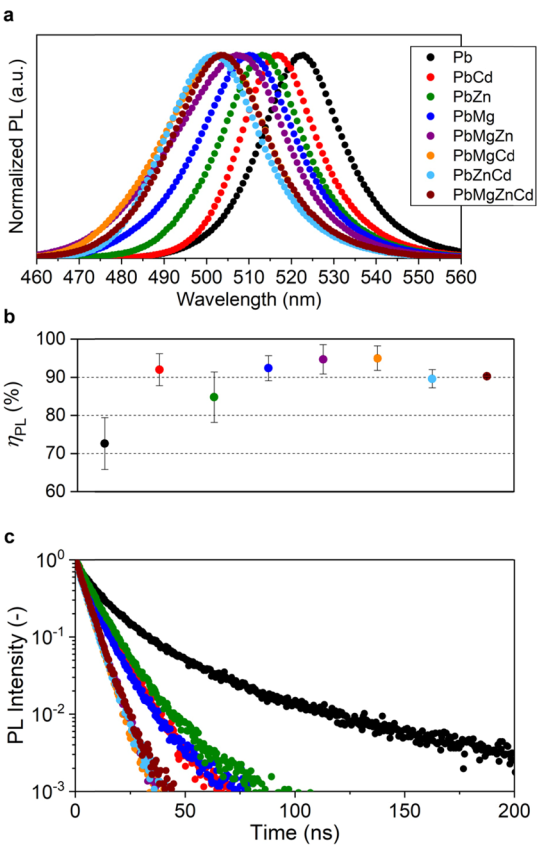

Figure 2. Emission characteristics of HEP NCs. (a) PL spectra, (b) η_{PL}, and (c) PL lifetime for bare $MAPbBr_3$ NCs, single-doped perovskite NCs, and HEP NCs, showing emission blueshift together with an enhanced PL quantum yield and reduced lifetime upon high-entropy alloying.

https://doi.org/10.1021/jacs.1c12294
J. Am. Chem. Soc. 2022, 144, 5864−5870

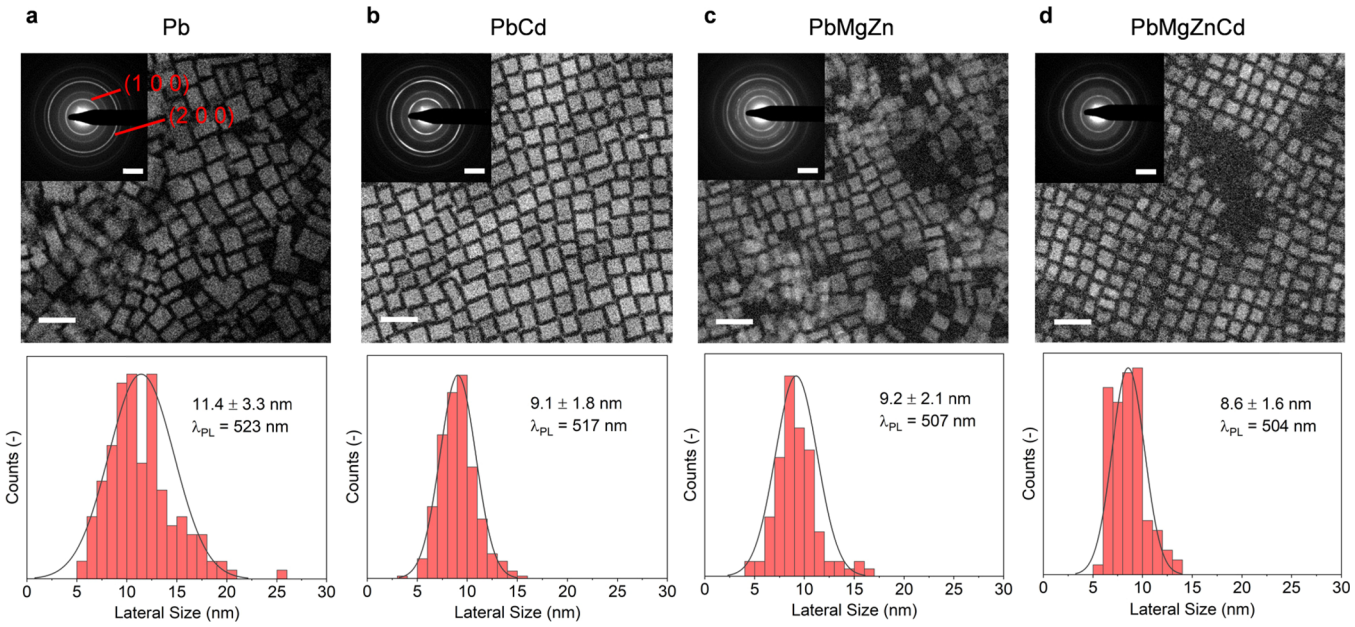

Figure 3. Structural characterization of HEP NCs. Cryo-STEM images, electron diffraction patterns, and corresponding size distribution graphs for (a) parent $MAPbBr_3$, (b) $MA(PbCd)Br_3$, (c) $MA(PbMgZn)Br_3$, and (d) $MA(PbMgZnCd)Br_3$ NCs, revealing that the NC shape, morphology, and crystallography are preserved upon alloying. Scale bars: 20 nm for STEM images and 2 nm^{-1} for ED patterns.

lifetime becomes shorter when more secondary elements are involved, with the exception of $MA(PbMgZnCd)Br_3$ HEP NCs. These results are of practical interest because fluorophores with high η_{PL} and low τ_{avg} are desirable for most photonic applications. In general, our results suggest that high-entropy alloying does not compromise the NC optical performance, but rather enhances it. For the detailed values for the characterized optical properties, please see Supplementary Table S1.

Clearly, the mechanism responsible for the enhanced optical properties is beyond a simple picture of defect passivation, in which the enhancement of η_{PL} comes with an elongated PL lifetime.[49,50] For B-site doping (or Pb replacement), it has been reported that the incorporation of divalent metal cations could give a shorter lifetime.[32] In the HEP NCs, the lifetime can be further shortened to 5 ns, which is significantly shorter than that of the single-doped systems, confirming that high-entropy B-site doping stabilizes the LHP structure with a higher degree of Pb replacement.

We attribute the observed enhancement of emission characteristics upon alloying to the nature of intrinsic and surface defects and their interactions with metal cations.[50−52] First, the divalent cations could rectify these intrinsic defects by occupying the vacancies within the crystal lattice, thereby increasing the short-range ordering in perovskite lattices.[25,33] Second, the shallow surface trap states, which are responsible for the delayed fluorescence in perovskite NCs, were passivated by the metal and bromide ions, as reflected by the shortened lifetime and enhanced η_{PL}.[53] The entropy of mixing certainly plays a role in defect passivation, as more secondary elements are involved; shorter lifetimes are observed, but the exact mechanisms remain unclear. Interestingly, when bare $PbBr_2$ was used as the solid source in the LASPS reaction, instead of defect passivation, the parent $MAPbBr_3$ NCs were fragmented to form nanoplatelets (NPLs),[54] yielding a blueshift of the PL emission and a strong excitonic peak in the absorption spectra directly after the synthesis (Supplementary Figure S2), whereas complete dissolution of parent $MAPbBr_3$ NCs was observed if the reaction is performed without any metal bromide salts (Supplementary Figure S3).

We further investigated the colloidal stability of the synthesized HEP NCs by monitoring the solution optical density (OD) and η_{PL} with time (Supplementary Figure S4). For all samples considered here, the solution OD remained nearly unchanged within one month. Their η_{PL} values are also very stable, except that of $MA(PbZnCd)Br_3$ and $MA(PbMgZnCd)Br_3$ HEP samples, which gradually decreased by approximately 10%, whereas η_{PL} remarkably enhanced by approximately 10% for bare $MAPbBr_3$ NCs over a period of one month. Overall, the colloidal stability of the HEP NCs is comparable to that of the parent $MAPbBr_3$ NCs. The strong fluorescence properties of the colloidal NC dispersions are preserved upon a storage time of one year, demonstrating their excellent colloidal and shelf stability (Supplementary Figure S5).

Figure 3 presents the cryo-scanning transmission electron microscopy (cryo-STEM) images and the corresponding size distribution graphs of the NCs, revealing that the NC shape and morphology are preserved upon alloying (also see Supplementary Figure S6). The insets show the corresponding electron diffraction (ED) patterns. For each sample, the two most intense diffraction rings, corresponding to (100) and (200) lattice planes, were preserved. In other words, the cubic crystalline structure of parent $MAPbBr_3$ NCs is preserved. The size analysis reveals a small degree of size reduction for the metal-doped perovskite NCs. Specifically, metal-doped perovskite NCs have an average lateral size of ~9 ± 2 nm, which is about 2 nm smaller as compared to parent $MAPbBr_3$ NCs (~11 ± 3 nm). A similar degree of size reduction has also been observed for B-site-doped perovskite NCs synthesized via the hot-injection technique with mixed precursors.[55] The difference in the size could result from the use of surfactants during the metal-doping process, whose polar nature is known to cause a degree of NC size reduction to quantum-confined

https://doi.org/10.1021/jacs.1c12294
J. Am. Chem. Soc. 2022, 144, 5864−5870

matter.[56] Although the metal-doped NCs possess similar sizes, they exhibit different PL emission wavelengths (λ_{PL}). In addition, there is a lack of extensive excitonic absorption features in the absorption spectra of the metal-doped perovskite NCs (Supplementary Figure S1), agreeing that the size of the NCs remains far larger than the excitonic Bohr radius, which is known to be ~2 nm for $MAPbBr_3$.[56,57] Overall, the small degree of size reduction of the single-doped NCs and the HEP NCs alone would not result in the considerable blueshift of the PL emission wavelength observed.

We carried out more crystallographic analysis for the drop-casted films using the powder X-ray diffraction (XRD) goniometer and the grazing-incidence wide-angle X-ray scattering (GIWAXS) at a synchrotron light source. Analogous to the ED patterns, the XRD patterns show two main peaks corresponding to the (100) and (200) lattice planes (Supplementary Figure S7). We determine the unit cell parameter a = 5.9311(21) Å for the parent $MAPbBr_3$ cubic phase, consistent with the literature.[58,59] The detailed crystallographic parameters are presented in Supplementary Table S2.

As for the HEP NCs, the XRD and GIWAXS patterns revealed a more complex picture. Because all the secondary elements considered here, Mg^{2+}, Zn^{2+}, and Cd^{2+}, have smaller ionic radius than Pb^{2+}, one would expect to see a degree of lattice contraction upon alloying.[19] As expected for samples of nanosized crystallites, the reflections that originate from the perovskite NCs are very broad and also very weak for reflections at higher angles, which hampered the precise determination of the peak positions. No significant change in the average lattice parameter a could be detected, revealing the complex nature of high-entropy alloying in colloidal perovskite NCs. The emergence of low-angle peaks in the XRD patterns could originate from the formation of layered structures (see Supplementary Table S3).[60] These findings are consistent with low-angle reflections in the GIWAXS patterns (Supplementary Figure S8). Furthermore, the formation of assembly structures during the high-entropy alloying process is suggested (scanning electron microscopy (SEM) image; see Supplementary Figure S9).

We further looked into the synchrotron GIWAXS patterns, which offer significantly higher resolution than benchtop XRD. Figure 4 magnifies the (100) plane peaks extracted from the GIWAXS patterns, revealing a clear trend that the diffraction peak becomes more asymmetric and multicomponent when more secondary elements are involved. We fitted each pattern with multicomponent Lorentzians according to the number of secondary elements involved in the system. Given the excellent agreement with the measured data, our observations are summarized as follows: (i) upon alloying, two sets of diffractive components emerge; one shift toward higher wavenumbers and the other toward lower wavenumbers, as compared to the parent $MAPbBr_3$ peak, (ii) when more secondary elements are involved, components with a higher degree of wavenumber shifts are attained; for example, for $MA(PbMgZnCd)Br_3$ HEP NCs, components centered at q = 10.10 and 11.07 nm^{-1}, corresponding to d-spacings of 6.22 and 5.67 Å were resolved, or remarkably ~5.0% expansion and ~4.5% contraction, and (iii) the summation of all components can therefore yield a peak maximum shifting to lower or higher wavenumbers.

Accordingly, the crystallographic evidence presented here elucidates the effects of high-entropy alloying on perovskite NCs. First, similar to many high-entropy alloy metallurgical

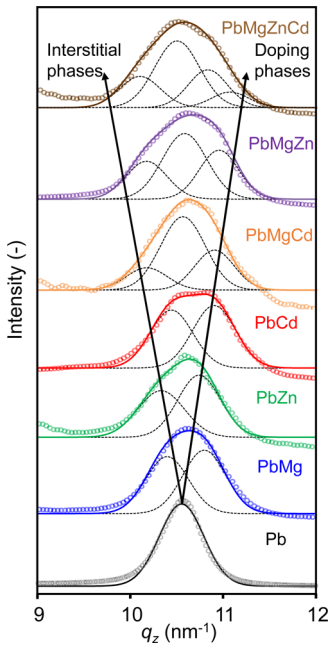

Figure 4. Synchrotron X-ray scattering analysis of HEP NCs. Magnified (100) plane peaks extracted from the GIWAXS patterns of bare $MAPbBr_3$, single-doped perovskite NCs, and HEP NCs, where the dots correspond to the measured data, and the solid curves are their multicomponent fittings, with individual Lorentzians represented in dashed lines. The arrows highlight the emergence of doping (lattice contraction) and interstitial (lattice expansion) phases. When more secondary elements were added, the phases with higher degrees of lattice expansion and lattice contraction were stabilized.

systems,[35,36] the HEP NC systems are multiphase systems rather than single-phase, solid solutions. Second, alloying with more than one secondary element results in the emergence of lattice expansion phases. Here, we term these phases the "interstitial phases," as the smaller secondary elements can occupy some of the spaces within the perovskite lattices, yielding lattice expansion.[61] On the other hand, we refer the "doping phases" to the lattice contraction phases, in which the lead sites were replaced by the secondary elements (see the arrows in Figure 4).[32,62] Third, most importantly, when more secondary elements were added, the phases with higher degrees of lattice expansion and lattice contraction were stabilized. The important findings promise the stabilization of "lead-reduced" phases upon high-entropy alloying.

We systematically carried out energy-dispersive X-ray spectroscopy (EDXS) in a scanning electron microscope for the semiquantitative analysis of the elemental composition of the parent $MAPbBr_3$ NCs, single-doped perovskite NCs, and HEP NCs (Supplementary Figures S10 and S11). Figure 5 presents the characterized atomic ratios of Br to Pb (left axis) and Br to the sum of Pb and M (right axis) for all samples considered here. The Br/Pb ratio for parent $MAPbBr_3$ NCs is 3.49 ± 0.06. Remarkably, there exists a trend that the Br/Pb ratio increases with the number of secondary elements, increasing up to 7.31 ± 0.87 for $MA(PbZnCd)Br_3$ NCs and 7.56 ± 1.95 for $MA(PbMgZnCd)Br_3$ NCs. In other words, the lead content is approximately reduced by 55% upon high-entropy alloying. On the other hand, the Br/(Pb + M) ratios for most HEP NCs are slightly below 3, the ideal perovskite stoichiometry, independent of the number of secondary elements. We attribute the reduced Br/(Pb + M) ratios in

https://doi.org/10.1021/jacs.1c12294
J. Am. Chem. Soc. 2022, 144, 5864−5870

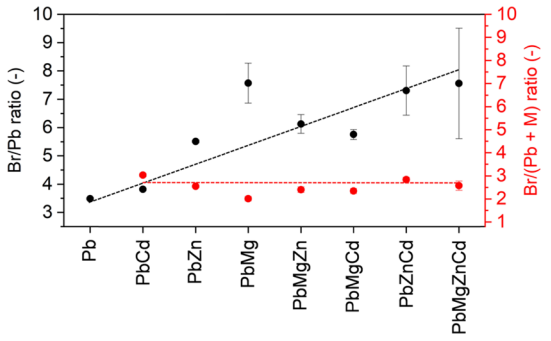

Figure 5. Reduced lead contents in the HEP NCs. The characterized Br/Pb (black dots) and Br/(Pb + M) (M = Mg^{2+}, Zn^{2+}, and Cd^{2+}) ratios (red dots) from the EDXS analysis reveal a high degree of reduction in perovskite lead content by increasing the number of secondary elements.

HEP NCs to the formation of interstitial phases, echoing our findings in Figure 4. We notice that the composition heterogeneity for HEP NC systems with more than two secondary elements, such as $MA(PbZnCd)Br_3$ and $MA(PbMgZnCd)Br_3$ HEP NCs, is relatively high, as reflected by the increased error bars. It may suggest a degree of phase segregation during the formation of the HEP NCs, for which advanced nanometer-scale characterization would be required. In addition, there is an outlier, $MA(PbMg)Br_3$, having an unusually high Br/Pb ratio because of the fact that the EDXS peak for Mg K transition is very close to that for Br L transition at an energy of ~1.254 keV.[63,64] This issue becomes less considerable for other HEP NC systems because their Mg content is relatively low.

Finally, the protocol presented here also worked for Mn^{2+} doping, yielding a strong blueshift of the emission wavelength to 486 nm. Additionally, a broad and weak PL shoulder peaking around 600 nm is visible (Supplementary Figure S12), which corresponds to the nominally forbidden Mn^{2+} d−d transition.[65] The low PL intensity of the Mn^{2+} d−d transition can be attributed to an ineffective exciton energy transfer between the bromide-based perovskite donor material and the Mn^{2+} acceptor.[22] Because a different emission mechanism is involved, we did not include it in our HEP analysis.

CONCLUSIONS

In summary, we report an approach to synthesize an interesting class of lead-reduced perovskite NCs, the HEP NCs. With a reduction of lead of up to 55%, the HEP NCs remain to possess excellent optical properties and colloidal stability. According to our crystallographic analysis, the formation of interstitial and doping phases upon high-entropy alloying is responsible for the stabilization of lead-reduced perovskite lattices. Although we report the usage of Cd, we anticipate the concept of high-entropy alloying presented here will open an avenue toward less-toxic and more environmentally friendly materials, which are strongly desirable for future device applications.

ASSOCIATED CONTENT

Supporting Information

The Supporting Information is available free of charge at https://pubs.acs.org/doi/10.1021/jacs.1c12294.

Experimental section, absorption and additional PL spectra, stability measurements, additional photographs of the colloidal solutions under UV excitation, additional STEM images with corresponding size distribution graphs, additional electron diffraction patterns, XRD patterns, GIWAXS patterns, SEM image, EDXS analysis, PL characteristics including carrier lifetimes, and crystallographic parameters (PDF)

AUTHOR INFORMATION

Corresponding Author

Chih-Jen Shih − *Institute for Chemical and Bioengineering, ETH Zürich, 8093 Zürich, Switzerland;* orcid.org/0000-0002-5258-3485; Email: chih-jen.shih@chem.ethz.ch

Authors

Simon F. Solari − *Institute for Chemical and Bioengineering, ETH Zürich, 8093 Zürich, Switzerland;* orcid.org/0000-0002-9874-1485

Lok-Nga Poon − *Institute for Chemical and Bioengineering, ETH Zürich, 8093 Zürich, Switzerland*

Michael Wörle − *Laboratory of Inorganic Chemistry, ETH Zürich, 8093 Zürich, Switzerland*

Frank Krumeich − *Laboratory of Inorganic Chemistry, ETH Zürich, 8093 Zürich, Switzerland;* orcid.org/0000-0001-5625-1536

Yen-Ting Li − *Department of Chemical Engineering, National Taiwan University of Science and Technology, Taipei 10607, Taiwan; National Synchrotron Radiation Research Center, Hsinchu 30076, Taiwan*

Yu-Cheng Chiu − *Department of Chemical Engineering, National Taiwan University of Science and Technology, Taipei 10607, Taiwan; Advanced Research Center for Green Materials Science and Technology, National Taiwan University, Taipei 10617, Taiwan;* orcid.org/0000-0003-4812-5681

Complete contact information is available at: https://pubs.acs.org/10.1021/jacs.1c12294

Author Contributions

#S.F.S. and L-N.P. contributed equally.

Notes

The authors declare no competing financial interest.

ACKNOWLEDGMENTS

The authors are grateful for the financial support from the Swiss National Science Foundation (project number: 200021-178944). We thank Dr. K. Kunze for helpful discussions and technical assistance with the EDXS measurements. The authors thank Dr. S. Matveev and G. Raggl from JEOL in Freising, Germany for SEM support. We thank G. Stemmler for assistance with the PL measurements. The authors are grateful to ScopeM (ETH Zürich) for access to the electron microscopy facilities.

REFERENCES

(1) Dey, A.; Ye, J.; De, A.; Debroye, E.; Ha, S. K.; Bladt, E.; Kshirsagar, A. S.; Wang, Z.; Yin, J.; Wang, Y.; Quan, L. N.; Yan, F.; Gao, M.; Li, X.; Shamsi, J.; Debnath, T.; Cao, M.; Scheel, M. A.; Kumar, S.; Steele, J. A.; Gerhard, M.; Chouhan, L.; Xu, K.; Wu, X.-G.; Li, Y.; Zhang, Y.; Dutta, A.; Han, C.; Vincon, I.; Rogach, A. L.; Nag, A.; Samanta, A.; Korgel, B. A.; Shih, C.-J.; Gamelin, D. R.; Son, D. H.; Zeng, H.; Zhong, H.; Sun, H.; Demir, H. V.; Scheblykin, I. G.; Mora-Seró, I.; Stolarczyk, J. K.; Zhang, J. Z.; Feldmann, J.; Hofkens, J.; Luther, J. M.; Pérez-Prieto, J.; Li, L.; Manna, L.; Bodnarchuk, M. I.;

https://doi.org/10.1021/jacs.1c12294
J. Am. Chem. Soc. 2022, 144, 5864−5870

Kovalenko, M. V.; Roeffaers, M. B. J.; Pradhan, N.; Mohammed, O. F.; Bakr, O. M.; Yang, P.; Müller-Buschbaum, P.; Kamat, P. V.; Bao, Q.; Zhang, Q.; Krahne, R.; Galian, R. E.; Stranks, S. D.; Bals, S.; Biju, V.; Tisdale, W. A.; Yan, Y.; Hoye, R. L. Z.; Polavarapu, L. State of the Art and Prospects for Halide Perovskite Nanocrystals. *ACS Nano* **2021**, *15*, 10775−10981.

(2) Akkerman, Q. A.; Rainò, G.; Kovalenko, M. V.; Manna, L. Genesis, challenges and opportunities for colloidal lead halide perovskite nanocrystals. *Nat. Mater.* **2018**, *17*, 394−405.

(3) Shamsi, J.; Urban, A. S.; Imran, M.; De Trizio, L.; Manna, L. Metal Halide Perovskite Nanocrystals: Synthesis, Post-Synthesis Modifications, and Their Optical Properties. *Chem. Rev.* **2019**, *119*, 3296−3348.

(4) Swarnkar, A.; Marshall, A. R.; Sanehira, E. M.; Chernomordik, B. D.; Moore, D. T.; Christians, J. A.; Chakrabarti, T.; Luther, J. M. Quantum dot-induced phase stabilization of alpha-CsPbI3 perovskite for high-efficiency photovoltaics. *Science* **2016**, *354*, 92−95.

(5) Akkerman, Q. A.; Gandini, M.; Di Stasio, F.; Rastogi, P.; Palazon, F.; Bertoni, G.; Ball, J. M.; Prato, M.; Petrozza, A.; Manna, L. Strongly emissive perovskite nanocrystal inks for high-voltage solar cells. *Nat. Energy* **2016**, *2*, 16194.

(6) Yang, T.; Zheng, Y.; Du, Z.; Liu, W.; Yang, Z.; Gao, F.; Wang, L.; Chou, K.-C.; Hou, X.; Yang, W. Superior Photodetectors Based on All-Inorganic Perovskite CsPbI3 Nanorods with Ultrafast Response and High Stability. *ACS Nano* **2018**, *12*, 1611−1617.

(7) Kim, Y.-H.; Kim, S.; Kakekhani, A.; Park, J.; Park, J.; Lee, Y.-H.; Xu, H.; Nagane, S.; Wexler, R. B.; Kim, D.-H.; Jo, S. H.; Martínez-Sarti, L.; Tan, P.; Sadhanala, A.; Park, G.-S.; Kim, Y.-W.; Hu, B.; Bolink, H. J.; Yoo, S.; Friend, R. H.; Rappe, A. M.; Lee, T.-W. Comprehensive defect suppression in perovskite nanocrystals for high-efficiency light-emitting diodes. *Nat. Photonics* **2021**, *15*, 148−155.

(8) Kumar, S.; Jagielski, J.; Marcato, T.; Solari, S. F.; Shih, C.-J. Understanding the Ligand Effects on Photophysical, Optical, and Electroluminescent Characteristics of Hybrid Lead Halide Perovskite Nanocrystal Solids. *J. Phys. Chem. Lett.* **2019**, *10*, 7560−7567.

(9) Hassan, Y.; Park, J. H.; Crawford, M. L.; Sadhanala, A.; Lee, J.; Sadighian, J. C.; Mosconi, E.; Shivanna, R.; Radicchi, E.; Jeong, M.; Yang, C.; Choi, H.; Park, S. H.; Song, M. H.; De Angelis, F.; Wong, C. Y.; Friend, R. H.; Lee, B. R.; Snaith, H. J. Ligand-engineered bandgap stability in mixed-halide perovskite LEDs. *Nature* **2021**, *591*, 72−77.

(10) Liu, M.; Wan, Q.; Wang, H.; Carulli, F.; Sun, X.; Zheng, W.; Kong, L.; Zhang, Q.; Zhang, C.; Zhang, Q.; Brovelli, S.; Li, L. Suppression of temperature quenching in perovskite nanocrystals for efficient and thermally stable light-emitting diodes. *Nat. Photonics* **2021**, *15*, 379−385.

(11) Solari, S. F.; Kumar, S.; Jagielski, J.; Shih, C.-J. Monochromatic LEDs based on perovskite quantum dots: Opportunities and challenges. *J. Soc. Inf. Disp.* **2019**, *27*, 667−678.

(12) Wong, A. B.; Bekenstein, Y.; Kang, J.; Kley, C. S.; Kim, D.; Gibson, N. A.; Zhang, D.; Yu, Y.; Leone, S. R.; Wang, L.-W.; Alivisatos, A. P.; Yang, P. Strongly Quantum Confined Colloidal Cesium Tin Iodide Perovskite Nanoplates: Lessons for Reducing Defect Density and Improving Stability. *Nano Lett.* **2018**, *18*, 2060−2066.

(13) Huang, J.; Lei, T.; Siron, M.; Zhang, Y.; Yu, S.; Seeler, F.; Dehestani, A.; Quan, L. N.; Schierle-Arndt, K.; Yang, P. Lead-free Cesium Europium Halide Perovskite Nanocrystals. *Nano Lett.* **2020**, *20*, 3734−3739.

(14) Infante, I.; Manna, L. Are There Good Alternatives to Lead Halide Perovskite Nanocrystals? *Nano Lett.* **2021**, *21*, 6−9.

(15) Jellicoe, T. C.; Richter, J. M.; Glass, H. F. J.; Tabachnyk, M.; Brady, R.; Dutton, S. E.; Rao, A.; Friend, R. H.; Credgington, D.; Greenham, N. C.; Böhm, M. L. Synthesis and Optical Properties of Lead-Free Cesium Tin Halide Perovskite Nanocrystals. *J. Am. Chem. Soc.* **2016**, *138*, 2941−2944.

(16) Kang, C.; Rao, H.; Fang, Y.; Zeng, J.; Pan, Z.; Zhong, X. Antioxidative Stannous Oxalate Derived Lead-Free Stable CsSnX3 (X = Cl, Br, and I) Perovskite Nanocrystals. *Angew. Chem., Int. Ed.* **2021**, *60*, 660−665.

(17) Shen, X.; Zhang, Y.; Kershaw, S. V.; Li, T.; Wang, C.; Zhang, X.; Wang, W.; Li, D.; Wang, Y.; Lu, M.; Zhang, L.; Sun, C.; Zhao, D.; Qin, G.; Bai, X.; Yu, W. W.; Rogach, A. L. Zn-Alloyed CsPbI3 Nanocrystals for Highly Efficient Perovskite Light-Emitting Devices. *Nano Lett.* **2019**, *19*, 1552−1559.

(18) Liu, H.; Wu, Z.; Shao, J.; Yao, D.; Gao, H.; Liu, Y.; Yu, W.; Zhang, H.; Yang, B. CsPbxMn1−xCl3 Perovskite Quantum Dots with High Mn Substitution Ratio. *ACS Nano* **2017**, *11*, 2239−2247.

(19) Das, S.; De, A.; Samanta, A. Ambient Condition Mg2+ Doping Producing Highly Luminescent Green- and Violet-Emitting Perovskite Nanocrystals with Reduced Toxicity and Enhanced Stability. *J. Phys. Chem. Lett.* **2020**, *11*, 1178−1188.

(20) Zhou, Y.; Chen, J.; Bakr, O. M.; Sun, H.-T. Metal-Doped Lead Halide Perovskites: Synthesis, Properties, and Optoelectronic Applications. *Chem. Mater.* **2018**, *30*, 6589−6613.

(21) Luo, B.; Li, F.; Xu, K.; Guo, Y.; Liu, Y.; Xia, Z.; Zhang, J. Z. B-Site doped lead halide perovskites: synthesis, band engineering, photophysics, and light emission applications. *J. Mater. Chem. C* **2019**, *7*, 2781−2808.

(22) Liu, W.; Lin, Q.; Li, H.; Wu, K.; Robel, I.; Pietryga, J. M.; Klimov, V. I. Mn2+-Doped Lead Halide Perovskite Nanocrystals with Dual-Color Emission Controlled by Halide Content. *J. Am. Chem. Soc.* **2016**, *138*, 14954−14961.

(23) Imran, M.; Ramade, J.; Di Stasio, F.; De Franco, M.; Buha, J.; Van Aert, S.; Goldoni, L.; Lauciello, S.; Prato, M.; Infante, I.; Bals, S.; Manna, L. Alloy CsCdxPb1−xBr3 Perovskite Nanocrystals: The Role of Surface Passivation in Preserving Composition and Blue Emission. *Chem. Mater.* **2020**, *32*, 10641−10652.

(24) Wang, H.-C.; Wang, W.; Tang, A.-C.; Tsai, H.-Y.; Bao, Z.; Ihara, T.; Yarita, N.; Tahara, H.; Kanemitsu, Y.; Chen, S.; Liu, R.-S. High-Performance CsPb1−xSnxBr3 Perovskite Quantum Dots for Light-Emitting Diodes. *Angew. Chem., Int. Ed.* **2017**, *56*, 13650−13654.

(25) Yong, Z.-J.; Guo, S.-Q.; Ma, J.-P.; Zhang, J.-Y.; Li, Z.-Y.; Chen, Y.-M.; Zhang, B.-B.; Zhou, Y.; Shu, J.; Gu, J.-L.; Zheng, L.-R.; Bakr, O. M.; Sun, H.-T. Doping-Enhanced Short-Range Order of Perovskite Nanocrystals for Near-Unity Violet Luminescence Quantum Yield. *J. Am. Chem. Soc.* **2018**, *140*, 9942−9951.

(26) Milstein, T. J.; Kroupa, D. M.; Gamelin, D. R. Picosecond Quantum Cutting Generates Photoluminescence Quantum Yields Over 100% in Ytterbium-Doped CsPbCl3 Nanocrystals. *Nano Lett.* **2018**, *18*, 3792−3799.

(27) Yao, J.-S.; Ge, J.; Han, B.-N.; Wang, K.-H.; Yao, H.-B.; Yu, H.-L.; Li, J.-H.; Zhu, B.-S.; Song, J.-Z.; Chen, C.; Zhang, Q.; Zeng, H.-B.; Luo, Y.; Yu, S.-H. Ce3+-Doping to Modulate Photoluminescence Kinetics for Efficient CsPbBr3 Nanocrystals Based Light-Emitting Diodes. *J. Am. Chem. Soc.* **2018**, *140*, 3626−3634.

(28) Cai, T.; Yang, H.; Hills-Kimball, K.; Song, J.-P.; Zhu, H.; Hofman, E.; Zheng, W.; Rubenstein, B. M.; Chen, O. Synthesis of All-Inorganic Cd-Doped CsPbCl3 Perovskite Nanocrystals with Dual-Wavelength Emission. *J. Phys. Chem. Lett.* **2018**, *9*, 7079−7084.

(29) Pan, G.; Bai, X.; Yang, D.; Chen, X.; Jing, P.; Qu, S.; Zhang, L.; Zhou, D.; Zhu, J.; Xu, W.; Dong, B.; Song, H. Doping Lanthanide into Perovskite Nanocrystals: Highly Improved and Expanded Optical Properties. *Nano Lett.* **2017**, *17*, 8005−8011.

(30) Begum, R.; Parida, M. R.; Abdelhady, A. L.; Murali, B.; Alyami, N. M.; Ahmed, G. H.; Hedhili, M. N.; Bakr, O. M.; Mohammed, O. F. Engineering Interfacial Charge Transfer in CsPbBr3 Perovskite Nanocrystals by Heterovalent Doping. *J. Am. Chem. Soc.* **2017**, *139*, 731−737.

(31) Gao, D.; Qiao, B.; Xu, Z.; Song, D.; Song, P.; Liang, Z.; Shen, Z.; Cao, J.; Zhang, J.; Zhao, S. Postsynthetic, Reversible Cation Exchange between Pb2+ and Mn2+ in Cesium Lead Chloride Perovskite Nanocrystals. *J. Phys. Chem. C* **2017**, *121*, 20387−20395.

(32) van der Stam, W.; Geuchies, J. J.; Altantzis, T.; van den Bos, K. H. W.; Meeldijk, J. D.; Van Aert, S.; Bals, S.; Vanmaekelbergh, D.; de Mello Donega, C. Highly Emissive Divalent-Ion-Doped Colloidal

https://doi.org/10.1021/jacs.1c12294
J. Am. Chem. Soc. 2022, 144, 5864−5870

CsPb1−xMxBr3 Perovskite Nanocrystals through Cation Exchange. *J. Am. Chem. Soc.* **2017**, *139*, 4087−4097.
(33) Mondal, N.; De, A.; Samanta, A. Achieving Near-Unity Photoluminescence Efficiency for Blue-Violet-Emitting Perovskite Nanocrystals. *ACS Energy Lett.* **2019**, *4*, 32−39.
(34) Nedelcu, G.; Protesescu, L.; Yakunin, S.; Bodnarchuk, M. I.; Grotevent, M. J.; Kovalenko, M. V. Fast Anion-Exchange in Highly Luminescent Nanocrystals of Cesium Lead Halide Perovskites (CsPbX3, X = Cl, Br, I). *Nano Lett.* **2015**, *15*, 5635−5640.
(35) Miracle, D. B.; Senkov, O. N. A critical review of high entropy alloys and related concepts. *Acta Mater.* **2017**, *122*, 448−511.
(36) George, E. P.; Raabe, D.; Ritchie, R. O. High-entropy alloys. *Nat. Rev. Mater.* **2019**, *4*, 515−534.
(37) Ye, Y. F.; Wang, Q.; Lu, J.; Liu, C. T.; Yang, Y. High-entropy alloy: challenges and prospects. *Mater. Today* **2016**, *19*, 349−362.
(38) Kumar, S.; Jagielski, J.; Tian, T.; Kallikounis, N.; Lee, W.-C.; Shih, C.-J. Mixing Entropy-Induced Layering Polydispersity Enabling Efficient and Stable Perovskite Nanocrystal Light-Emitting Diodes. *ACS Energy Lett.* **2019**, *4*, 118−125.
(39) Yi, C.; Luo, J.; Meloni, S.; Boziki, A.; Ashari-Astani, N.; Grätzel, C.; Zakeeruddin, S. M.; Röthlisberger, U.; Grätzel, M. Entropic stabilization of mixed A-cation ABX3 metal halide perovskites for high performance perovskite solar cells. *Energy Environ. Sci.* **2016**, *9*, 656−662.
(40) Jiang, S.; Hu, T.; Gild, J.; Zhou, N.; Nie, J.; Qin, M.; Harrington, T.; Vecchio, K.; Luo, J. A new class of high-entropy perovskite oxides. *Scr. Mater.* **2018**, *142*, 116−120.
(41) Sarkar, A.; Djenadic, R.; Wang, D.; Hein, C.; Kautenburger, R.; Clemens, O.; Hahn, H. Rare earth and transition metal based entropy stabilised perovskite type oxides. *J. Eur. Ceram. Soc.* **2018**, *38*, 2318−2327.
(42) Sharma, Y.; Musico, B. L.; Gao, X.; Hua, C.; May, A. F.; Herklotz, A.; Rastogi, A.; Mandrus, D.; Yan, J.; Lee, H. N.; Chisholm, M. F.; Keppens, V.; Ward, T. Z. Single-crystal high entropy perovskite oxide epitaxial films. *Phys. Rev. Mater.* **2018**, *2*, No. 060404.
(43) Wang, T.; Chen, H.; Yang, Z.; Liang, J.; Dai, S. High-Entropy Perovskite Fluorides: A New Platform for Oxygen Evolution Catalysis. *J. Am. Chem. Soc.* **2020**, *142*, 4550−4554.
(44) Nguyen, T. X.; Liao, Y.-C.; Lin, C.-C.; Su, Y.-H.; Ting, J.-M. Advanced High Entropy Perovskite Oxide Electrocatalyst for Oxygen Evolution Reaction. *Adv. Funct. Mater.* **2021**, *31*, No. 2101632.
(45) Krawczyk, P. A.; Jurczyszyn, M.; Pawlak, J.; Salamon, W.; Baran, P.; Kmita, A.; Gondek, Ł.; Sikora, M.; Kapusta, C.; Strączek, T.; Wyrwa, J.; Żywczak, A. High-Entropy Perovskites as Multifunctional Metal Oxide Semiconductors: Synthesis and Characterization of (Gd0.2Nd0.2La0.2Sm0.2Y0.2)CoO3. *ACS Appl. Electron. Mater.* **2020**, *2*, 3211−3220.
(46) Solari, S. F.; Kumar, S.; Jagielski, J.; Kubo, N. M.; Krumeich, F.; Shih, C.-J. Ligand-assisted solid phase synthesis of mixed-halide perovskite nanocrystals for color-pure and efficient electroluminescence. *J. Mater. Chem. C* **2021**, *9*, 5771−5778.
(47) Loiudice, A.; Segura Lecina, O.; Bornet, A.; Luther, J. M.; Buonsanti, R. Ligand Locking on Quantum Dot Surfaces via a Mild Reactive Surface Treatment. *J. Am. Chem. Soc.* **2021**, *143*, 13418−13427.
(48) Huang, G.; Wang, C.; Xu, S.; Zong, S.; Lu, J.; Wang, Z.; Lu, C.; Cui, Y. Postsynthetic Doping of MnCl2 Molecules into Preformed CsPbBr3 Perovskite Nanocrystals via a Halide Exchange-Driven Cation Exchange. *Adv. Mater.* **2017**, *29*, No. 1700095.
(49) Di Stasio, F.; Christodoulou, S.; Huo, N.; Konstantatos, G. Near-Unity Photoluminescence Quantum Yield in CsPbBr3 Nanocrystal Solid-State Films via Postsynthesis Treatment with Lead Bromide. *Chem. Mater.* **2017**, *29*, 7663−7667.
(50) Bodnarchuk, M. I.; Boehme, S. C.; ten Brinck, S.; Bernasconi, C.; Shynkarenko, Y.; Krieg, F.; Widmer, R.; Aeschlimann, B.; Günther, D.; Kovalenko, M. V.; Infante, I. Rationalizing and Controlling the Surface Structure and Electronic Passivation of Cesium Lead Halide Nanocrystals. *ACS Energy Lett.* **2019**, *4*, 63−74.
(51) Seth, S.; Ahmed, T.; De, A.; Samanta, A. Tackling the Defects, Stability, and Photoluminescence of CsPbX3 Perovskite Nanocrystals. *ACS Energy Lett.* **2019**, *4*, 1610−1618.
(52) Ye, J.; Byranvand, M. M.; Martínez, C. O.; Hoye, R. L. Z.; Saliba, M.; Polavarapu, L. Defect Passivation in Lead-Halide Perovskite Nanocrystals and Thin Films: Toward Efficient LEDs and Solar Cells. *Angew. Chem., Int. Ed.* **2021**, *60*, 21636−21660.
(53) Li, F.; Liu, Y.; Wang, H.; Zhan, Q.; Liu, Q.; Xia, Z. Postsynthetic Surface Trap Removal of CsPbX3 (X = Cl, Br, or I) Quantum Dots via a ZnX2/Hexane Solution toward an Enhanced Luminescence Quantum Yield. *Chem. Mater.* **2018**, *30*, 8546−8554.
(54) Jagielski, J.; Solari, S. F.; Jordan, L.; Scullion, D.; Blülle, B.; Li, Y.-T.; Krumeich, F.; Chiu, Y.-C.; Ruhstaller, B.; Santos, E. J. G.; Shih, C.-J. Scalable photonic sources using two-dimensional lead halide perovskite superlattices. *Nat. Commun.* **2020**, *11*, 387.
(55) Chen, J.-K.; Ma, J.-P.; Guo, S.-Q.; Chen, Y.-M.; Zhao, Q.; Zhang, B.-B.; Li, Z.-Y.; Zhou, Y.; Hou, J.; Kuroiwa, Y.; Moriyoshi, C.; Bakr, O. M.; Zhang, J.; Sun, H.-T. High-Efficiency Violet-Emitting All-Inorganic Perovskite Nanocrystals Enabled by Alkaline-Earth Metal Passivation. *Chem. Mater.* **2019**, *31*, 3974−3983.
(56) Kumar, S.; Jagielski, J.; Yakunin, S.; Rice, P.; Chiu, Y.-C.; Wang, M.; Nedelcu, G.; Kim, Y.; Lin, S.; Santos, E. J. G.; Kovalenko, M. V.; Shih, C.-J. Efficient Blue Electroluminescence Using Quantum-Confined Two-Dimensional Perovskites. *ACS Nano* **2016**, *10*, 9720−9729.
(57) Tanaka, K.; Takahashi, T.; Ban, T.; Kondo, T.; Uchida, K.; Miura, N. Comparative study on the excitons in lead-halide-based perovskite-type crystals CH3NH3PbBr3 CH3NH3PbI3. *Solid State Commun.* **2003**, *127*, 619−623.
(58) Liu, Y.; Yang, Z.; Cui, D.; Ren, X.; Sun, J.; Liu, X.; Zhang, J.; Wei, Q.; Fan, H.; Yu, F.; Zhang, X.; Zhao, C.; Liu, S. Two-Inch-Sized Perovskite CH3NH3PbX3 (X = Cl, Br, I) Crystals: Growth and Characterization. *Adv. Mater.* **2015**, *27*, 5176−5183.
(59) Wang, K.-H.; Li, L.-C.; Shellaiah, M.; Wen Sun, K. Structural and Photophysical Properties of Methylammonium Lead Tribromide (MAPbBr3) Single Crystals. *Sci. Rep.* **2017**, *7*, 13643.
(60) Stoumpos, C. C.; Cao, D. H.; Clark, D. J.; Young, J.; Rondinelli, J. M.; Jang, J. I.; Hupp, J. T.; Kanatzidis, M. G. Ruddlesden−Popper Hybrid Lead Iodide Perovskite 2D Homologous Semiconductors. *Chem. Mater.* **2016**, *28*, 2852−2867.
(61) Phung, N.; Félix, R.; Meggiolaro, D.; Al-Ashouri, A.; Sousa e Silva, G.; Hartmann, C.; Hidalgo, J.; Köbler, H.; Mosconi, E.; Lai, B.; Gunder, R.; Li, M.; Wang, K.-L.; Wang, Z.-K.; Nie, K.; Handick, E.; Wilks, R. G.; Marquez, J. A.; Rech, B.; Unold, T.; Correa-Baena, J.-P.; Albrecht, S.; De Angelis, F.; Bär, M.; Abate, A. The Doping Mechanism of Halide Perovskite Unveiled by Alkaline Earth Metals. *J. Am. Chem. Soc.* **2020**, *142*, 2364−2374.
(62) Yang, Z.; Wei, M.; Voznyy, O.; Todorovic, P.; Liu, M.; Quintero-Bermudez, R.; Chen, P.; Fan, J. Z.; Proppe, A. H.; Quan, L. N.; Walters, G.; Tan, H.; Chang, J.-W.; Jeng, U. S.; Kelley, S. O.; Sargent, E. H. Anchored Ligands Facilitate Efficient B-Site Doping in Metal Halide Perovskites. *J. Am. Chem. Soc.* **2019**, *141*, 8296−8305.
(63) Newbury, D. E.; Ritchie, N. W. M. Performing elemental microanalysis with high accuracy and high precision by scanning electron microscopy/silicon drift detector energy-dispersive X-ray spectrometry (SEM/SDD-EDS). *J. Mater. Sci.* **2015**, *50*, 493−518.
(64) Newbury, D. E.; Ritchie, N. W. M. Is Scanning Electron Microscopy/Energy Dispersive X-ray Spectrometry (SEM/EDS) Quantitative? *Scanning* **2013**, *35*, 141−168.
(65) Guria, A. K.; Dutta, S. K.; Adhikari, S. D.; Pradhan, N. Doping Mn2+ in Lead Halide Perovskite Nanocrystals: Successes and Challenges. *ACS Energy Lett.* **2017**, *2*, 1014−1021.

https://doi.org/10.1021/jacs.1c12294
J. Am. Chem. Soc. 2022, 144, 5864−5870